J Nanopart Res (2023) 25:1
https://doi.org/10.1007/s11051-022-05649-3

RESEARCH PAPER

High specific surface area niobium-doped tin oxide nanoparticles produced in spray flames as catalyst supports in polymer electrolyte fuel cells

Tomoyuki Hirano · Takama Tsuboi · Kiet Le Anh Cao · Eishi Tanabe · Takashi Ogi

Received: 30 June 2022 / Accepted: 6 December 2022

Abstract Platinum-loaded carbon is commonly used in polymer electrolyte fuel cells (PEFCs); however, it is known to corrode or degrade under high potentials, which results in poor cell performance. Niobium-doped tin oxide (Nb-SnO_2; NTO) nanoparticles are alternative materials to carbon because of their high durability and good cell performance as catalyst support in fuel cells. Here, we introduce the preparation of NTO nanoparticles with high specific surface area by spray flames. The particle characteristics and PEFC performances of the nanoparticles were evaluated. Spray combustion with a two-fluid nozzle was used where the raw material species were rapidly gasified to form fine nanoparticles. The spray flame synthesis was operated at a combustion enthalpy density of 4.87 kJ/g_{gas}. This enabled homogeneous nanoparticle formation and suppressed particle growth under a minimal condition. The flame-made NTO nanoparticles showed a primary particle size and specific surface area of ~ 8.77 nm and 87.04 m^2/g, respectively. Rietveld analysis revealed a detailed crystal structure of the NTO nanoparticles. In addition, Pt was loaded on the NTO nanoparticles and the cell performance of the resulting material was assessed using a membrane electrode assembly. The results of this study can be used to improve the features of flame-made NTO nanoparticles in order to suit the needs of a fuel cell application.

Keywords Nb-doped SnO_2 · Fuel cell · Electrocatalyst · Flame spray pyrolysis · Spray flame · NTO nanoparticles · Self-assembly

Supplementary information The online version contains supplementary material available at https://doi.org/10.1007/s11051-022-05649-3.

This article is part of the topical collection: "*Self-assembled Functional Nanomaterials and Devices in Asia*"

Guest Editors: Zhixiang Wei and Yong Yan

T. Hirano (✉) · T. Tsuboi · K. L. A. Cao · T. Ogi (✉)
Chemical Engineering Program, Graduate School of Advanced Science and Engineering, Hiroshima University, 1-4-1 Kagamiyama, Higashi Hiroshima, Hiroshima 739-8527, Japan
e-mail: tomoyuki-hirano@hiroshima-u.ac.jp

T. Ogi
e-mail: ogit@hiroshima-u.ac.jp

E. Tanabe
Hiroshima Prefectural Institute of Industrial Science and Technology, 3-13-26 Kagamiyama, Higashi Hiroshima, 739-0046 Hiroshima, Japan

Introduction

Polymer electrolyte fuel cells (PEFCs) convert directly the chemical energy from hydrogen fuel into electrical energy, resulting in a high-power generation efficiency [1–5]. In the research and development of a next-generation power generation system with low environmental impact, rapid progress has been aimed

Published online: 17 December 2022

at the installation of PEFCs in ordinary automobiles. However, to achieve wider applications in heavy-duty vehicles that require long-distance driving, it is vital to improve the durability of an electrode catalyst [6]. An approach to improve the durability of electrode catalysts is to develop metal-oxide catalyst support materials [7].

Carbon black (CB) with high specific surface area and high conductivity has been used as a carrier for conventional PEFCs. However, CB is easily degraded by corrosion under high temperatures, high potentials, and acidic conditions. Metal oxides (e.g., Nb-doped SnO_2 (NTO) nanoparticles) that exhibit excellent stability under such conditions have attracted attention as catalyst support materials [8–10]. NTO nanoparticles loaded with platinum have been reported to provide good durability against voltage cycling using high potentials [11, 12].

Among the methods proposed for the synthesis of NTO nanoparticles as catalyst supports for PEFCs, the flame method has received attention since it can provide particles with a structure that is required in high-performance catalyst supports [13–15]. In this combustion synthesis method in the gas phase, the raw material is rapidly gasified by combustion. The nanoparticles are then obtained by rapid cooling in the gas phase [16]. Pure oxygen is often used as the oxidant; thus, the flame temperature could be ≥ 2000 °C, which causes the fusion between primary particles and the formation of nanoparticle aggregates with a network structure [17–19]. The resulting aggregates improve gas diffusion, electronic conductivity of a support, and surface area in catalyst layers when the catalyst particles are incorporated into a fuel cell [10, 13, 14, 20–22]. To introduce the excellent features of flame-made NTOs for practical use, the preparation of NTO nanoparticles with high specific surface area in sufficiently large quantities is critical.

We have recently synthesized Pt-NTO nanoparticles by spray flame synthesis with the aid of a two-fluid nozzle [15]. Compared to previously reported droplet generation processes such as ultrasonic atomization [23–25] and electrostatic atomization [26, 27], the two-fluid nozzle atomizes the raw material solution at a higher throughput [28–31]. It has been demonstrated in practical trials as a nanoparticle production method. Meanwhile, in the formation of ceramic oxide particles by spray flame synthesis, homogeneous nanoparticles were obtained at high combustion enthalpy densities when the solvent boiling point (T_{bp}) was smaller than the melting point of a metal precursor (T_{mp}) [32]. A direct relationship between combustion enthalpy density and particle size was observed. In this study, NTO nanoparticles with a high specific surface area were prepared by spray flame synthesis using the two-fluid nozzle under minimum combustion enthalpy density to obtain homogeneous nanoparticles. The particle characteristics of the prepared material were also investigated in detail.

Experimental

Preparation of catalyst

NTO nanoparticles were synthesized by the flame spray pyrolysis method. $C_{16}H_{30}O_4Sn$ (92.5–100% purity) and $Nb(OC_2H_5)_5$ (99.95% purity) were obtained from Sigma-Aldrich Co. (state, USA). They were dissolved in xylene (≥ 98.5% purity) from Sigma-Aldrich Co. to prepare the precursor solution. The total concentration of Sn and Nb was 0.1 mol/L (Nb was 4 atom%). The solution was transported by a syringe pump to a two-fluid nozzle model AM6 from ATOMAX Co. (Shizuoka, Japan) at a flow rate of 3 mL/min and sprayed with oxygen (1.5 L/min). The atomized solution was ignited by a methane (CH_4)/air premixed flame (CH_4 and air at 1.2 and 10 L/min, respectively) to form a spray flame. The produced particles were collected using a polytetrafluoroethylene (PTFE) membrane filter from HORKOS Corp. (Hiroshima, Japan). Details of the apparatus are shown in a previous report [15]. Ten weight percent or 20 wt% of Pt nanoparticles was loaded on the NTO by the liquid-phase reduction method. Functionalization of the NTO nanoparticles was conducted by Pt deposition on the NTO surfaces through a liquid-phase reduction method. First, 2.0 g of NTO nanoparticles was suspended in 50 g of ultrapure water and stirred at 250 rpm for 30 min. Next, an appropriate amount of hexahydroxoplatinum amine solution was slowly added dropwise to the NTO suspension, and the mixture was stirred for 30 min. This solution was heated with continued stirring to stabilize the temperature at 95 °C. Then, the reducing agent was slowly added drop by drop to the NTO suspension. Afterward, the solution was washed with ultrapure water and filtered through a membrane filter, which was

then dried in an oven at 80 °C for 12 h to obtain Pt-loaded NTO (Pt/NTO) catalyst powder. The obtained 10 wt% or 20 wt% Pt-loaded NTO particles is denoted 10 or 20 NTO.

Characterization

The morphologies of the prepared particles were examined using field-emission scanning electron microscopy (FE-SEM) using a S-5200 model instrument from Hitachi High-Tech. Corp. (Tokyo, Japan) and transmission electron microscopy (TEM) using a 297-kV JEM-3000F model instrument from JEOL Ltd. (Tokyo, Japan). The crystal structures of the particles were investigated by x-ray powder diffraction (XRD) using a D2 PHASER model instrument from Bruker Corp. (Billerica, MA, USA) which was operated at 40 kV and 30 mA. Structure refinements were performed using the Rietveld method by the computer program RIETAN-FP [33]. Crystallite size was determined by the Halder-Wagner method [34, 35]. X-ray photoelectron spectroscopy (XPS) analysis was performed using an ESCA-3400 instrument model from Shimadzu Corp. (Kyoto, Japan), which was operated at 10 kV and 20 mA. The energy dependence was calibrated using the C 1 s spectrum. Background subtraction was done using the Shirley method. The specific surface areas were determined from the nitrogen adsorption–desorption isotherms obtained at 77 K using a BELSORP-max instrument model from BEL Japan (Osaka, Japan). The Nb K-edge X-ray absorption near-edge structures (XANES) were obtained at the BL11S2 beamline at Aichi SR. A sample and boron nitride were mixed in a mortar for 30 min before being pressed into a thin disk with a diameter of 10 mm. A disk was set in a holder. The measurements were performed in transmission mode in air.

Electrochemical measurements

The catalyst inks for the cathodes were made by mixing the Pt/NTO catalyst, Nafion ionomer from Wako Pure Chemical Industries Ltd. (Osaka, Japan), ethanol, and purified water using a homogenizer with an ionomer/support (I/S) volume ratio of 0.175. The Pt loading amount of the cathodes was 0.1 mg/cm^2. Pt/C (Pt loading 20 wt%; Ketjen black ECP; Lion Specialty Chemicals Co., Ltd., Tokyo, Japan) was used for all anodes in the test cells. A commercial carbon-supported (XC-72R, Cabot Corporation, Waltham, MA, USA) Pt catalyst was used for reference for the cathode measurements. The catalyst inks for the anodes were prepared similarly. For the anode electrode, the Pt loading and I/S were around 0.1 mg/cm^2 and 1.0, respectively. The membrane electrode assembly (MEA) was prepared using a decal transfer technique, which involved hot-pressing the anode and cathode catalyst layers that were coated on PTFE sheets onto a Nafion membrane at a temperature and pressure of 126 °C and 10 MPa, respectively. The geometric area of the electrodes was 1.0 cm^2. The MEA was placed in a home-made single cell holder with straight-line gas flow channels. The cell potential as a function of current density was measured at a cell temperature and relative humidity of 60 °C and 100%, respectively. Hydrogen gas and air was introduced to the anode and cathode, respectively. The back pressures for the cathode and anode were 108 kPa. The gas flow rates at the cathode and anode were 1.0 and 0.5 L/min, respectively. The pre-conditioning process was carried out before main measurements. The pre-conditioning processes were performed at 0.1 V/s between 0 and 1.0 V for 40 cycles. The AC-impedance measurements were also carried out from 100 kHz to 0.1 Hz with a potential of 0.4 V and an amplitude of 0.02 V. Cells and MEAs were the same as for the output measurement. Temperature, humidity, and back pressure were the same as for the output measurement, but measurements were conducted under non-power generation conditions. The current–voltage curves were potentionstatically measured at 0.01 V/s between 0 and 1.0 V. The cyclic voltammetry (CV) with a reversible hydrogen electrode as the reference electrode was performed to evaluate the electrochemical characteristics. The electrochemical measurement steps and conditions for CV are described elsewhere [15, 36].

Results and discussion

NTO nanoparticles were prepared by flame spray pyrolysis. The fine particles formed in the spray flame are shown in Fig. 1a. The self-sustaining spray flame is formed by atomizing precursor droplets containing Nb and Sn raw materials with a two-fluid nozzle. The droplets are continuously ignited with a pilot flame. The combustion proceeded stably without extinction

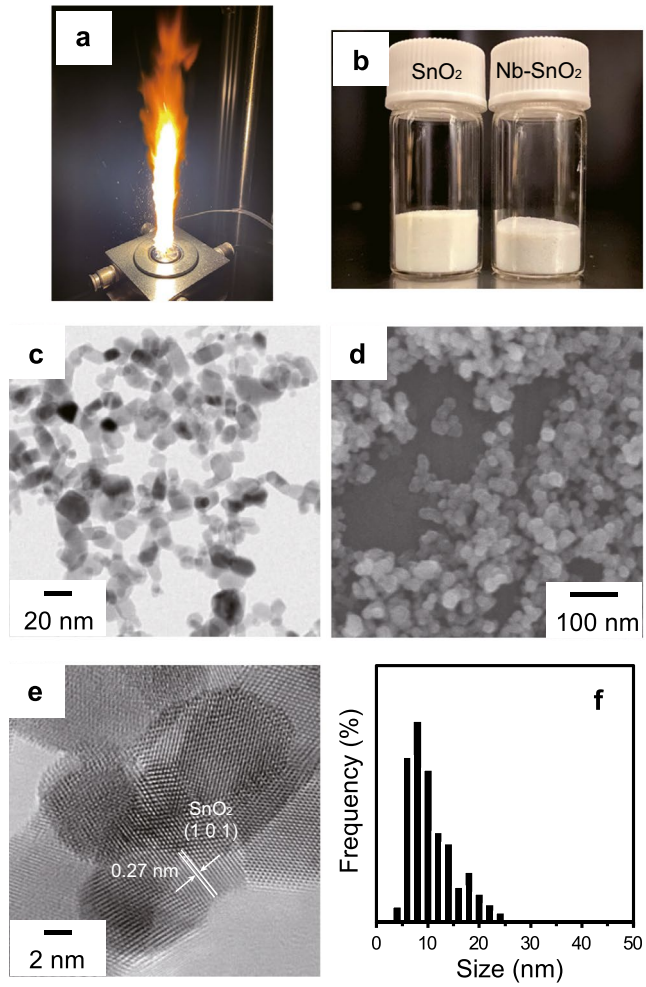

Fig. 1 (**a**) Spray flame in this study. (**b**) Appearance of tin oxide (SnO_2) and niobium-doped SnO_2 (Nb-SnO_2). (**c**) Transmission electron microscopy (TEM), (**d**) scanning electron microscopy (SEM), (**e**) high-resolution-TEM (HR-TEM) images, and (**f**) particle size distribution of Nb-SnO_2

and a white NTO powder was obtained. The appearance of the SnO_2 and NTO powders is shown in Fig. 1b. Both powders were white in color. No change in powder appearance was observed due to the Nb doping. The TEM and SEM images of the synthesized NTO nanoparticles are shown in Fig. 1c and d. The aggregation structure of the NTO nanoparticles was similar to carbon that is used in fuel cell catalysts [37]. When nanoparticles are synthesized by spray flames, the rapid heating and cooling processes in the high-temperature field of the flame typically produce particles with a necking structure with primary particles that are fused together. The HR-TEM images in Fig. 1e show lattice fringes (spacing = 0.27 nm) that originate from the (1 0 1) planes of the rutile structure SnO_2, confirming the high crystallinity of the nanoparticles. The atomic diameter of Nb is 0.64 Å, which is the same as Sn (0.69 Å); thus, no lattice defects or changes in lattice constants were observed. The Ferret diameter was approximated from the NTO nanoparticle TEM images. The particle size distribution obtained is shown in Fig. 1f. Particle size measurements were performed on > 500 particles. The geometric mean diameter (d_p) and geometric standard deviation (σ_g) were 8.77 nm and 1.57, respectively. These suggested relatively uniform and fine nanoparticles were obtained. The specific surface area from the nitrogen adsorption test was 87.04 m^2/g. The primary particle size (d_{BET}) calculated using the density of SnO_2 (6.95 g/cm^3) was 9.92 nm. The adsorption isotherms and pore size distribution by nitrogen adsorption are shown in Fig. S1 of the Supporting Information (SI). The calculated combustion enthalpy density was 4.87 kJ/g_{gas}. According to previous studies [32], when spray flame synthesis is performed with combustion enthalpy density of

4.7 kJ/g at $T_{bp}/T_{mp} < 1.05$, sufficient heat is provided to the precursor to form homogeneous nanoparticles. Under the combustion enthalpy density in this study, the minimum condition for homogeneous nanoparticle formation was achieved and no extra heat was provided, resulting in the smaller nanoparticles formation. Compared to NTO nanoparticles synthesized by the liquid phase method (~30 m^2/g) [8] and the flame oxide-synthesis method (31 m^2/g) [10], our nanoparticles showed a much larger specific surface area of 604.92 m^2/cm^3_{SnO2} (by volume). This value is also 2× larger than the conventional graphitized CB (~300 m^2/cm^3_{Carbon}) [38, 39].

X-ray absorption spectroscopy was conducted to identify the state of Nb species. The XANES results of the synthesized NTO nanoparticles near the Nb K-edge are shown in Fig. S2 of the SI. The XANES spectrum showed a white line at around 19,020 eV, which is similar to the reference Nb_2O_5. This suggested that the present Nb species in the synthesized material were Nb^{5+}. The electrical conductivity of SnO_2 is significantly increased by doping with hypervalent cations like Nb^{5+} or Sb^{5+} [40, 41]. The Nb^{5+} doping into SnO_2 introduces more electrons in the conduction band. The Nb^{5+} cation acts as an n-type dopant of SnO_2 and might enhance the electrocatalytic activity related to charge transfer processes.

The Rietveld analysis of the prepared NTO nanoparticles is shown in Fig. 2. The crystallographic parameters of NTO obtained by XRD refinement are summarized in Table S1 of the SI. The refinement was performed using the crystal structure model $P4_2/mnm$ with reference to a previous study [42]. The final R factors represent the confidence level of the analysis. The values were $R_{wp} = 4.05\%$ ($S = 1.4368$), $R_B = 0.563\%$, and $R_F = 0.252\%$, which were sufficiently low to support the structure model. Although the added Nb^{5+} occupied some of the Sn^{4+} positions, no significant change in the lattice constant was observed. This was because the atomic radii of these ions are similar. To maintain charge neutrality during the addition of Nb^{5+}, free electrons are generated. These electrons contribute to the improved electronic conductivity of the NTO support. The crystallite size by the Halder-Wagner method was 8.70 nm, which is sufficiently close to the primary particle size, indicating that the synthesized nanoparticles are highly crystalline.

To use the prepared NTO nanoparticles as catalysts in PEFCs, Pt was loaded on the nanoparticles by a liquid phase method. The XRD patterns of the prepared Pt-loaded NTO nanoparticles are shown in Fig. 3. The Pt-loaded NTO (10 Pt/NTO and 20 Pt/NTO) showed broad peaks of Pt in a cubic structure. Diffraction peaks attributed to SnO_2 were also observed.

TEM was used to confirm the particle morphology of the Pt catalyst on the NTO support. The Pt nanoparticles (10 and 20 Pt/NTO) with size of ~3 nm were uniformly dispersed on the NTOs (Fig. 4a and c). The HR-TEM images of the 10 and 20 Pt/NTO samples are shown in Fig. 4b and d. The Pt nanoparticles on the

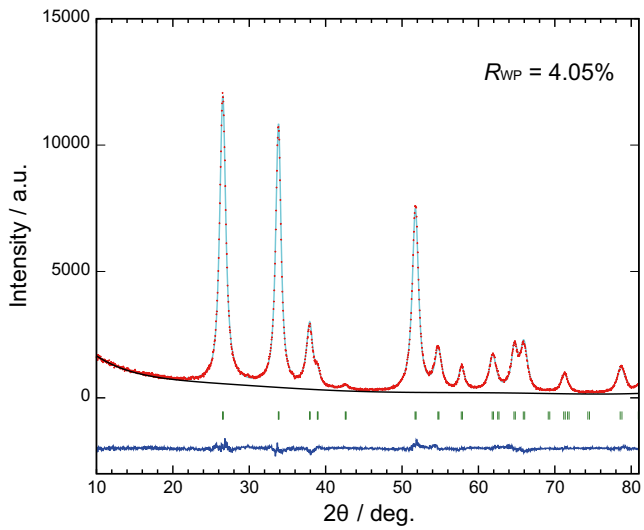

Fig. 2 Rietveld refinement result of the prepared niobium-doped tin oxide (NTO) nanoparticles

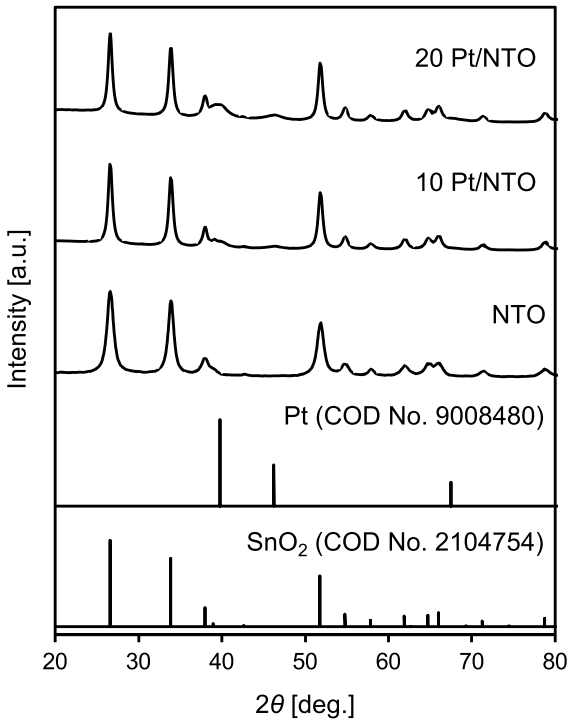

Fig. 3 X-ray powder diffraction patterns of the Pt-loaded NTO nanoparticles with different Pt contents

NTO surface in both samples showed a lattice spacing of 0.23 nm due to the Pt (1 1 1) plane. This indicated that both samples have uniform and high crystallinity. The TEM-EDS mapping of the samples is shown in Fig. S3 of the SI. The results also suggest that the support particles were uniformly distributed with Nb, Sn, and O on the formed NTO. The presence of Pt nanoparticles on the NTO support was confirmed.

The cyclic voltammograms of the 10 and 20 Pt/NTO samples and commercial Pt/C are shown in Fig. 5. The values that were calculated as the current divided by Pt mass in the catalyst layer are used on the *y*-axis. The current peaks in all samples, which correspond to the adsorption and desorption of hydrogen on Pt, were clearly observed in the potentials more negative than 0.3 V vs. RHE. The electrochemically active surface area (ECSA) values were 50.2 and 46.7 m^2/g-Pt for the 10 and 20 Pt/NTO samples, respectively. In the 20 wt% Pt loading, a large amount of Pt was present on the NTO support. The Pt nanoparticles were uniformly loaded on the nanoparticles without aggregation as suggested by the ECSA values and TEM results.

The I-V performance of MEAs, which were fabricated with Pt/NTO and commercial Pt/C cathode electrocatalysts, was evaluated using a single cell. The I-V performance of a single cell with a Pt/NTO catalyst layer has been shown to be improved when the volume ratio of Nafion®

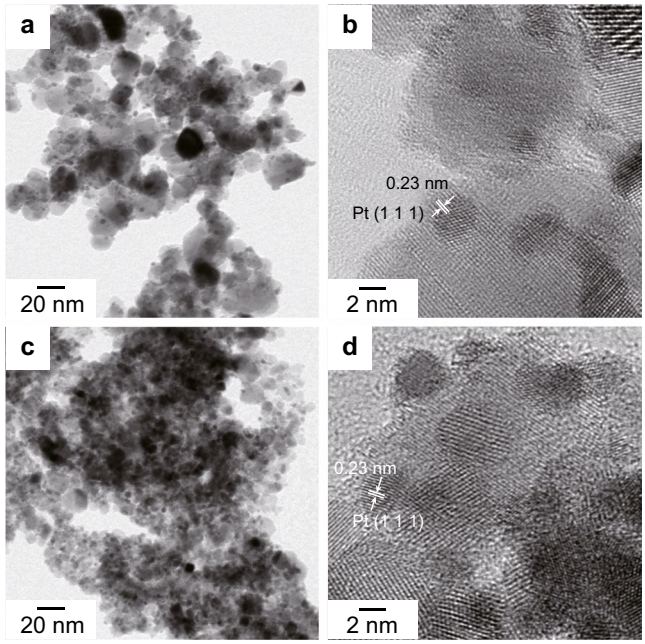

Fig. 4 Representative TEM and HR-TEM images of (**a** and **b**) 10 Pt/NTO and (**c** and **d**) 20 Pt/NTO samples

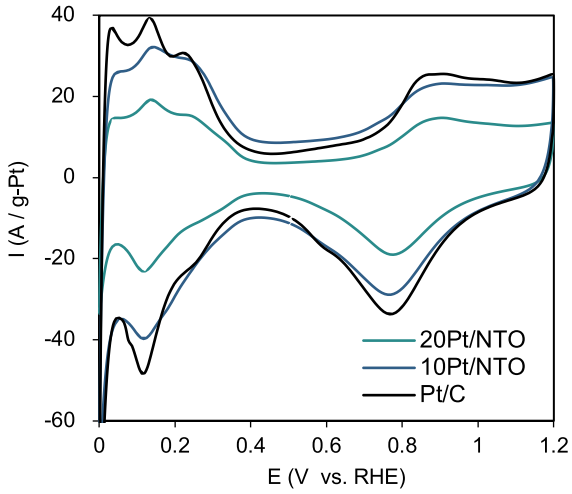

Fig. 5 Cyclic voltammogram of prepared Pt/NTO at different Pt mass loading and commercial Pt/C

ionomer to support (I/S) is < 0.24 [22]. Therefore, the I-V characteristics in very humid conditions with I/S of 0.175 were determined and the results are shown in Fig. 6a. The cell with 20 Pt/NTO showed a higher performance than the cell with 10 Pt/NTO. Representative cross-sectional SEM images of the catalyst layers with 10 and 20 Pt/NTO are shown in Fig. 6b and c. The catalyst layer thickness values were 2.5 and 1.6 µm for the 10 and 20 Pt/NTO samples, respectively. An increase in the Pt loading density most likely reduced the thickness of the catalyst layer, resulting in reduced gas diffusion and electronic resistances and better cell performance. Nyquist plots measured in a single cell using Pt/NTO at different Pt mass loading and commercial Pt/C are shown in Fig. S4 in the Supporting Information. The impedances of the cells using Pt/NTO are increased compared to the commercial Pt/C, but are decreased with increasing Pt loading density, which means decreasing proton resistances. The above results indicated that the prepared flame-made NTO nanoparticles are electrically conductive. The spray flame synthesis was also industrially feasible and produces particles with properties that can be precisely controlled by adjusting simple parameters (e.g., precursor flow rate, dispersed gas flow rate, and cooling rate). Therefore, the proposed technology shows potential for the high-volume and continuous manufacture of NTO nanoparticles with desirable electrical conductivities.

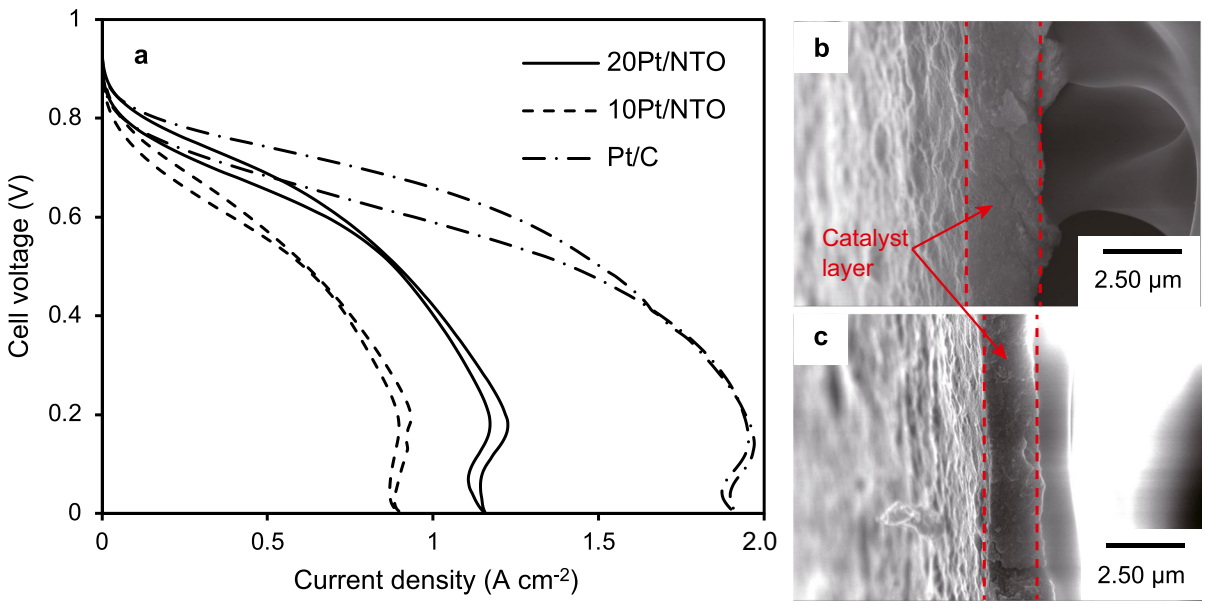

Fig. 6 (**a**) I-V characteristics of membrane electrode assemblies with 10 and 20 Pt/NTO and commercial Pt/C catalyst layers. Representative cross-sectional SEM images of (**b**) 10 and (**c**) 20 Pt/NTO samples

Conclusion

We successfully prepared NTO nanoparticles by spray flame synthesis with a two-fluid nozzle and characterized the properties of the nanoparticles. MEAs were fabricated with the NTO nanoparticles and their fuel cell performance was evaluated. Nb species were found to be present as Nb^{5+} in the NTO nanoparticles. Pt was loaded at 10 and 20 wt% on the NTO nanoparticles by a liquid phase method during the preparation of fuel cell catalysts. TEM studies confirmed that the Pt nanoparticles were uniformly dispersed on the NTO nanoparticles. Electrochemical characterization of the catalysts confirmed that the Pt nanoparticles maintained high ECSA values in the absence of particle aggregation even at high loading amounts. I-V measurements of MEAs fabricated with the flame-made Pt/NTO indicated an improved cell performance, which was caused by the high Pt loading amount to 20 wt%. This study improved our understanding of the characteristics of spray flame-made NTO nanoparticles for application in fuel cells.

Acknowledgements This work was partly supported by the Center for Functional Nano Oxides at Hiroshima University, the International Network on Polyoxometalate Science, the JSPS Core-to-Core Program. The authors thank the Natural Science Center for Basic Research and Development (N-BARD) for help with SEM image measurements.

Funding This work was supported by JSPS KAKENHI Grant Numbers JP22K20482 (T.H) and JP19H02500 (T.O.). This work was partly supported by the Information Center of Particle Technology, Japan, the Hosokawa Powder Technology Foundation, and the Kato Foundation for the Promotion of Science (KS-3229).

Declarations

Conflict of interest The authors declare no competing interests.

References

1. Kodama K, Nagai T, Kuwaki A, Jinnouchi R, Morimoto Y (2021) Challenges in applying highly active Pt-based nanostructured catalysts for oxygen reduction reactions to fuel cell vehicles. Nat Nanotechnol 16:140–147. https://doi.org/10.1038/s41565-020-00824-w
2. Jiao K, Xuan J, Du Q, Bao Z, Xie B, Wang B, Zhao Y, Fan L, Wang H, Hou Z, Huo S, Brandon NP, Yin Y, Guiver MD (2021) Designing the next generation of proton-exchange membrane fuel cells. Nature 595:361–369. https://doi.org/10.1038/s41586-021-03482-7
3. Staffell I, Scamman D, Velazquez Abad A, Balcombe P, Dodds PE, Ekins P, Shah N, Ward KR (2019) The role of hydrogen and fuel cells in the global energy system. Energy Environ Sci 12:463–491. https://doi.org/10.1039/c8ee01157e
4. Zhang J, Yuan Y, Gao L, Zeng G, Li M, Huang H (2021) Stabilizing Pt-based electrocatalysts for oxygen reduction reaction: fundamental understanding and design strategies. Adv Mater 33:e2006494. https://doi.org/10.1002/adma.202006494
5. Suter TAM, Smith K, Hack J, Rasha L, Rana Z, Angel GMA, Shearing PR, Miller TS, Brett DJL (2021) Engineering catalyst layers for next-generation polymer electrolyte fuel cells: a review of design, materials, and methods. Adv Energy Mater 11:2101025. https://doi.org/10.1002/aenm.202101025
6. Cullen DA, Neyerlin KC, Ahluwalia RK, Mukundan R, More KL, Borup RL, Weber AZ, Myers DJ, Kusoglu A (2021) New roads and challenges for fuel cells in heavy-duty transportation. Nat Energy 6:462–474. https://doi.org/10.1038/s41560-021-00775-z
7. Zhang Z, Liu J, Gu J, Su L, Cheng L (2014) An overview of metal oxide materials as electrocatalysts and supports for polymer electrolyte fuel cells. Energy Environ Sci 7:2535–2558. https://doi.org/10.1039/c3ee43886d
8. Takasaki F, Matsuie S, Takabatake Y, Noda Z, Hayashi A, Shiratori Y, Ito K, Sasaki K (2011) Carbon-free Pt electrocatalysts supported on SnO_2 for polymer electrolyte fuel cells: electrocatalytic activity and durability. J Electrochem Soc 158:B1270–B1275. https://doi.org/10.1149/1.3625918
9. Kakinuma K, Suda K, Kobayashi R, Tano T, Arata C, Amemiya I, Watanabe S, Matsumoto M, Imai H, Iiyama A, Uchida M (2019) Electronic states and transport phenomena of Pt nanoparticle catalysts supported on Nb-doped SnO_2 for polymer electrolyte fuel cells. ACS Appl Mater Interfaces 11:34957–34963. https://doi.org/10.1021/acsami.9b11119
10. Shi G, Tano T, Tryk DA, Iiyama A, Uchida M, Kakinuma K (2021) Temperature dependence of oxygen reduction activity at Pt/Nb-doped SnO_2 catalysts with varied Pt loading. ACS Catal 11:5222–5230. https://doi.org/10.1021/acscatal.0c05157
11. Matsumoto S, Nagamine M, Noda Z, Matsuda J, Lyth SM, Hayashi A, Sasaki K (2018) PEFC Electrocatalysts supported on Nb-SnO_2 for MEAs with high activity and durability: part II. Application of bimetallic Pt-alloy catalysts. J Electrochem Soc 165:F1164–F1175. https://doi.org/10.1149/2.0321814jes
12. Takei C, Kobayashi R, Mizushita Y, Hiramitsu Y, Kakinuma K, Uchida M (2018) Platinum anti-dissolution mechanism of Pt/Nb-SnO_2 cathode catalyst layer during load cycling in the presence of oxygen for polymer electrolyte fuel cells. J Electrochem Soc 165:F1300–F1311. https://doi.org/10.1149/2.0591816jes
13. Senoo Y, Kakinuma K, Uchida M, Uchida H, Deki S, Watanabe M (2014) Improvements in electrical and electrochemical properties of Nb-doped $SnO_{2-\delta}$ supports for

fuel cell cathodes due to aggregation and Pt loading. RSC Adv 4:32180–32188. https://doi.org/10.1039/c4ra03988b
14. Kakinuma K, Chino Y, Senoo Y, Uchida M, Kamino T, Uchida H, Deki S, Watanabe M (2013) Characterization of Pt catalysts on Nb-doped and Sb-doped $SnO_{2-\delta}$ support materials with aggregated structure by rotating disk electrode and fuel cell measurements. Electrochim Acta 110:316–324. https://doi.org/10.1016/j.electacta.2013.06.127
15. Hirano T, Tsuboi T, Tanabe E, Ogi T (2022) In-situ flame deposition of Pt catalysts on Nb-doped SnO_2 nanoparticles. J Alloys Compd 898:162749. https://doi.org/10.1016/j.jallcom.2021.162749
16. Li S, Ren Y, Biswas P, Tse SD (2016) Flame aerosol synthesis of nanostructured materials and functional devices: processing, modeling, and diagnostics. Prog Energy Combust Sci 55:1–59. https://doi.org/10.1016/j.pecs.2016.04.002
17. Teoh WY, Amal R, Madler L (2010) Flame spray pyrolysis: an enabling technology for nanoparticles design and fabrication. Nanoscale 2:1324–1347. https://doi.org/10.1039/c0nr00017e
18. Strobel R, Pratsinis SE (2007) Flame aerosol synthesis of smart nanostructured materials. J Mater Chem 17:4743–4756. https://doi.org/10.1039/b711652g
19. Pokhrel S, Madler L (2020) Flame-made particles for sensors, catalysis, and energy storage applications. Energy Fuels 34:13209–13224. https://doi.org/10.1021/acs.energyfuels.0c02220
20. Kakinuma K, Uchida M, Kamino T, Uchida H, Watanabe M (2011) Synthesis and electrochemical characterization of Pt catalyst supported on $Sn_{0.96}Sb_{0.04}O_{2-\delta}$ with a network structure. Electrochim Acta 56:2881–2887. https://doi.org/10.1016/j.electacta.2010.12.077
21. Chino Y, Kakinuma K, Tryk DA, Watanabe M, Uchida M (2015) Influence of Pt loading and cell potential on the HF ohmic resistance of an Nb-Doped SnO_2-supported Pt cathode for PEFCs. J Electrochem Soc 163:F97–F105. https://doi.org/10.1149/2.0571602jes
22. Kakinuma K, Kobayashi R, Iiyama A, Uchida M (2018) Influence of ionomer content on both cell performance and load cycle durability for polymer electrolyte fuel cells using Pt/Nb-SnO_2 cathode catalyst layers. J Electrochem Soc 165:J3083–J3089. https://doi.org/10.1149/2.0141815jes
23. Wang W-N, Purwanto A, Lenggoro IW, Okuyama K, Chang H, Jang HD (2008) Investigation on the correlations between droplet and particle size distribution in ultrasonic spray pyrolysis. Ind Eng Chem Res 47:1650–1659. https://doi.org/10.1021/ie070821d
24. Hirano T, Kikkawa J, Shimokuri D, Nandiyanto ABD, Ogi T (2021) Sinter-necked, mixed nanoparticles of metallic tungsten and tungsten oxide produced in fuel-rich methane/air tubular flames. J Chem Eng Jpn 54:557–565. https://doi.org/10.1252/jcej.21we009
25. Hirano T, Nakakura S, Rinaldi FG, Tanabe E, Wang W-N, Ogi T (2018) Synthesis of highly crystalline hexagonal cesium tungsten bronze nanoparticles by flame-assisted spray pyrolysis. Adv Powder Technol 29:2512–2520. https://doi.org/10.1016/j.apt.2018.07.001
26. Zaouk D, Zaatar Y, Khoury A, Llinares C, Charles JP, Bechara J (2000) Fabrication of tin oxide (SnO_2) thin film by electrostatic spray pyrolysis. Microelectron Eng 51–52:627–631. https://doi.org/10.1016/s0167-9317(99)00526-2
27. Chen C (1995) Fabrication of $LiCoO_2$ thin film cathodes for rechargeable lithium battery by electrostatic spray pyrolysis. Solid State Ionics 80:1–4. https://doi.org/10.1016/0167-2738(95)00140-2
28. Mueller R, Mädler L, Pratsinis SE (2003) Nanoparticle synthesis at high production rates by flame spray pyrolysis. Chem Eng Sci 58:1969–1976. https://doi.org/10.1016/s0009-2509(03)00022-8
29. Wegner K, Schimmöller B, Thiebaut B, Fernandez C, Rao TN (2011) Pilot plants for industrial nanoparticle production by flame spray pyrolysis. KONA Powder Part J 29:251–265. https://doi.org/10.14356/kona.2011025
30. Cao KLA, Iskandar F, Tanabe E, Ogi T (2022) Recent advances in the fabrication and functionalization of nanostructured carbon spheres for energy storage applications. KONA Powder Part J:2023016. https://doi.org/10.14356/kona.2023016
31. Gradon L, Balgis R, Hirano T, Rahmatika AM, Ogi T, Okuyama K. (2020) Advanced aerosol technologies towards structure and morphologically controlled next-generation catalytic materials. J Aerosol Sci 149:105608. https://doi.org/10.1016/j.jaerosci.2020.105608
32. Jossen R, Pratsinis SE, Stark WJ, Madler L (2005) Criteria for flame-spray synthesis of hollow, shell-like, or inhomogeneous oxides. J Am Ceram Soc 88:1388–1393. https://doi.org/10.1111/j.1551-2916.2005.00249.x
33. Izumi F, Momma K (2007) Three-dimensional visualization in powder diffraction. Solid State Phenom 130:15–20. https://doi.org/10.4028/www.scientific.net/SSP.130.15
34. Halder NC, Wagner CNJ (1966) Separation of particle size and lattice strain in integral breadth measurements. Acta Crystallogr A 20:312–313. https://doi.org/10.1107/s0365110x66000628
35. Halder NC, Wagner CNJ (1966) Analysis of the broadening of powder pattern peaks using variance, integral breadth, and Fourier coefficients of the line profile. Adv X-Ray Anal 9:91–102
36. Balgis R, Widiyastuti W, Ogi T, Okuyama K (2017) Enhanced electrocatalytic activity of Pt/3D hierarchical bimodal macroporous carbon nanospheres. ACS Appl Mater Interfaces 9:23792–23799. https://doi.org/10.1021/acsami.7b05873
37. Tang J, Liu J, Torad NL, Kimura T, Yamauchi Y (2014) Tailored design of functional nanoporous carbon materials toward fuel cell applications. Nano Today 9:305–323. https://doi.org/10.1016/j.nantod.2014.05.003
38. Bott-Neto JL, Asset T, Maillard F, Dubau L, Ahmad Y, Guérin K, Berthon-Fabry S, Mosdale A, Mosdale R, Ticianelli EA, Chatenet M (2018) Utilization of graphitized and fluorinated carbon as platinum nanoparticles supports for application in proton exchange membrane fuel cell cathodes. J Power Sources 404:28–38. https://doi.org/10.1016/j.jpowsour.2018.10.004

39. Asset T, Chattot R, Maillard F, Dubau L, Ahmad Y, Batisse N, Dubois M, Guérin K, Labbé F, Metkemeijer R, Berthon-Fabry S, Chatenet M (2018) Activity and durability of platinum-based electrocatalysts supported on bare or fluorinated nanostructured carbon substrates. J Electrochem Soc 165:F3346–F3358. https://doi.org/10.1149/2.031806jes
40. Gokulakrishnan V, Parthiban S, Jeganathan K, Ramamurthi K (2011) Investigations on the structural, optical and electrical properties of Nb-doped SnO2 thin films. J Mater Sci 46:5553–5558. https://doi.org/10.1007/s10853-011-5504-x
41. Szczuko D, Werner J, Oswald S, Behr G, Wetzig K (2001) XPS investigations of surface segregation of doping elements in SnO_2. Appl Surf Sci 179:301–306. https://doi.org/10.1016/s0169-4332(01)00298-7
42. Yamanaka T, Kurashima R, Mimaki J (2000) X-ray diffraction study of bond character of rutile-type SiO_2, GeO_2 and SnO_2. Z Kristallogr - Cryst Mater 215:424–428. https://doi.org/10.1524/zkri.2000.215.7.424